Iranian Polymer Journal (2021) 30:285–295
https://doi.org/10.1007/s13726-020-00890-w

ORIGINAL RESEARCH

Synthesis, characterization, optical, morphological, and antioxidant properties of oligo(2-ethoxy-6-(((2-hydroxyphenyl)imino)methyl) phenol) obtained by oxidative polycondensation

Esin Kaya[1] · Erman Erdoğan[2] · Ercan Bursal[3] · Erdal Canpolat[4]

Received: 26 July 2020 / Accepted: 1 December 2020 / Published online: 3 January 2021

Abstract
A newly designed oligo-Schiff-base was prepared and characterized to investigate its optical and morphological response and antioxidant activity. We first clarified the synthesis of 2-ethoxy-6-(((2-hydroxyphenyl)imino)methyl)phenol (EHPIMP) from the condensation reaction of 3-ethoxy-2-hydroxybenzaldehyde with 2-aminophenol. The subsequent oxidative polycondensation process yielded the target oligo(2-ethoxy-6-(((2-hydroxyphenyl)imino)-methyl)phenol), oligo (EHPIMP). The structural elucidation of oligo (EHPIMP) was performed by ^{1}H, ^{13}C NMR, TGA, FTIR and GPC systems. The optical properties of the EHPIMP and the oligo (EHPIMP)'s thin films were compared mainly with UV–Vis spectroscopy. Corresponding band gap (E_g) values of the EHPIMP and the oligo (EHPIMP) films were obtained as 2.224 and 1.404 eV, respectively. 2D and 3D surface images of films were analyzed with atomic force microscopy. In the AFM results, the surface roughness values and the average roughness were attained to be 8.28 nm and 46.63 nm for EHPIMP and the oligo (EHPIMP)'s thin films, respectively. Furthermore, the antioxidant activities were investigated using in vitro FRAP, CUPRAC, DPPH, and ABTS methods. The obtained data demonstrated that EHPIMP and oligo (EHPIMP) had effective reducing antioxidant potentials and radical scavenging activities.

Keywords Organic semiconductor · Poly-Schiff-base · Optical band gap · Morphology · Antioxidant · Radical scavenging · Thin films

Introduction

Nowadays, researchers attention has been shifted towaed an intensive search on the polycondensation reaction's products of Schiff-bases, labeled as a Schiff-base or a poly-Schiff-base depending on their chain sizes. Schiff-base derivatives are characterized by the presence of an azomethine group (–CH=N), and therefore, they are generally named as azomethine's or imine's [1]. Owing to their non-linear optical, electronic, electrochemical, antimicrobial, antiviral and anticancer activity properties, these advanced materials have been studied in divergent areas such as organic solar cells [2–4], detectors [5], photovoltaic [6], photostabilization [7], thermoelectric and thermo-stable [8, 9]. Also, Schiff-bases constitute a significant class of compounds used in pharmaceutical and medical field [10, 11]. The polymerization of Schiff-bases increases their fields of application. Poly-Schiff-bases have also found places in batteries, hydrometallurgy, and cation exchange resins [12–14], as well as in fireproof materials, adhesive for dental applications, and nuclear chemistry [15–17].

Schiff-bases and their polymers are conjugated materials being potential candidates for photovoltaic applications. Furthermore, the films of conjugated material have shown various superiorities for usages such as transistors, sensors and photovoltaic cells [18–20]. The thin films of conjugated materials significantly increase optical, mechanical and

✉ Erman Erdoğan
erman0702@gmail.com

[1] Department of Science, Faculty of Education, Muş Alparslan University, Muş, Turkey

[2] Electronic Communication Technology Program, Vocational High School, Bilecik Şeyh Edebali University, Bilecik, Turkey

[3] Department of Nursing, School of Health, Muş Alparslan University, Muş, Turkey

[4] Department of Chemistry, Faculty of Arts and Science, University of Firat, Elazığ, Turkey

electrical properties. In particular, these films have been used during the insulation and transmission coatings of the superconducting devices [21].

The band gap is known to be a very important parameter for photovoltaic device performances [22, 23]. Schiff-base's and their polymeric films with low band gap value can be the desirable materials for solar cell and optoelectronic devices owing to their chemical versatility, low weight, mechanical flexibility, ease of operation, wavelength adjustment and low-cost performance [24–27].

An organic semiconductor material, which is containing Schiff-base, is known to be very suitable for photonic applications due to its modulating, sensing and light-emitting properties. Also, films of the organic semiconductor are used on smart windows, energy conversion, and lasers [28–30] and as well as on solar cells and electronics areas [31–33]. Additionally, thanks to their optical properties, they have been employed in the manufacturing of optical discs and non-reflective and reflective coatings [34, 35].

Aromatic Schiff-bases with acceptor–donor groups by the expanded π-conjugated system and hydrogen-bonding network are promising as a class of organic compounds with a stable structure for electrical and technological applications. Conductivity and antioxidant properties of different aromatic Schiff-base polymers have been investigated related to their chemical structures for applications in the optical, electrical and biological fields [36]. Antioxidant activities of various Schiff-bases as DPPH, ABTS, and superoxide radical scavengers were reported in recent studies [37, 38]. In particular, it has been reported that the semiconductor action of these compounds improves by adding electron donor or electron attracting groups to the phenyl ring, and many compounds exhibit antioxidant activity [39–42].

In this article, we aimed to synthesis and characterization of the aromatic Schiff-base existing in the literature [43] and novel oligo-Schiff-base derivative, in the first part of the study. The oligo (EHPIMP) derived from 2-ethoxy-6-(((2-hydroxyphenyl)imino) methyl)-phenol was obtained. The structural determination of a novel oligo (EHPIMP) was determined by UV–Vis, ^{1}H NMR, ^{13}C NMR, TGA, FTIR and GPC techniques. In the second part, the optical properties of EHPIMP and oligo (EHPIMP)-coated films, including the detection of optical band gaps, absorbances and transmittance values, were investigated. The surface morphology of the EHPIMP and oligo (EHPIMP) films was analyzed by AFM. Moreover, the antioxidant activities of EHPIMP and oligo (EHPIMP) were determined by measuring their radical scavenging and reducing properties. For this purpose, ABTS cation radical scavenging, DPPH free radical scavenging, CUPRAC (cupric ions reducing antioxidant capacity), and FRAP (ferric ions reducing antioxidant power) in vitro methods were applied to the samples. BHA (butylated hydroxyanisole), BHT (butylated hydroxytoluene), α-tocopherol, trolox, and ascorbic acid, which are well-known antioxidant compounds [44], were used as standards for comparison.

Experimental

Starting materials

2-Aminophenol, 3-ethoxy-2-hydroxybenzaldehyde, potassium hydroxide (KOH), hydrochloric acid (HCl), dimethylformamide (DMF), ethanol, sodium hypochlorite (NaOCl) (10%) were supplied from Sigma Aldrich or Merck and were used without further purification for all experiments.

Equipment

The FTIR spectra were carried out by a Perkin Elmer spectrometer in the range of 4000–600 cm^{-1}. Agilent 1100 Series was used to determine the molecular weight and PDI of the oligo (EHPIMP) by gel permeation chromatography (GPC). An injection volume of 20 µL was used with an eluent (DMF) in a flow rate of 0.7 mL min^{-1}. Toluene was added as a flow maker. Poly(styrene) standards were used to calibrate for relative M_w and M_n (calibration range Mp 2500–270000 g/mol). The ultraviolet–visible (UV–Vis) spectrum was recorded at wavelength between 1100 and 190 nm at room temperature with a Shimadzu model UV-1800 Spectrophotometer. ^{1}H (400 MHz) and ^{13}C (100 MHz) NMR spectra were obtained in DMSO-d_6 solutions by Bruker DRX-400 high-performance digital FT-NMR spectrometer. TGA was performed using Perkin Elmer Pyris 1 in the range of room temperature to 800 °C with a heating rate of 10 °C min^{-1} under N_2 atmosphere.

Synthesis of EHPIMP

That monomer was synthesized according to literature in Scheme 1 [45] (yield: 41%, color: orange).

IR (ν, cm^{-1}): 1620 (CH=N), 1598 (aromatic C=C), 1438 (–C=C–N), 1275 (C–O); 3054, 2996, 2978 (aromatic C–H), 2869 (aliphatic C–H), ^{1}H NMR (400 MHz, DMSO-d_6) δ (ppm): 14.14 (s, 1H, OH), 9.82 (s, 1H, OH), 8.96 (s, 1H, –N=CH), 7.39–6.84 (m, 7H, Ar–C–H), 4.00 (OCH_3), 1.34 (CH_3) ^{13}C NMR (100 MHz, DMSO-d_6) δ (ppm): 162.00 (C=N), 152.38 (C–OH), 151.11, 147.80, 135.19, 128.58, 124.22, 119.64, 117.31, 116.94, (C atoms on aromatic ring), 63.99 (CH_2), 15.62 (CH_3).

Synthesis and characterization of the oligo (EHPIMP)

The (2-ethoxy-6-(((2-hydroxyphenyl)imino)methyl)phenol) (oligo (EHPIMP)) was synthesized by oxidative

Scheme 1 Preparation of the EHPIMP

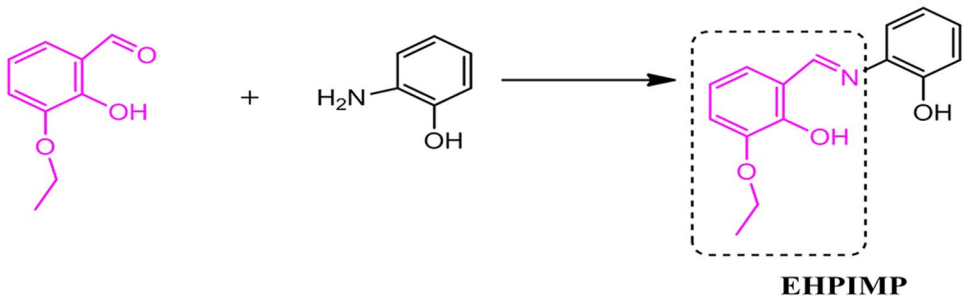

polycondensation adding NaOCl (10%) as oxidative reagent at 90 °C [46]. The EHPIMP (1.28 g, 5 mmol) was placed in two-necked vials equipped with a dropping funnel containing 10% NaOCI solution (12.1 mL, 10 mmol). DMF (12 mL) and KOH (7 mL) solution (0.56 g, 10 mmol) were added to the Schiff-base reagent, and the oxidative reagent was added dropwise to the reaction medium at 60 °C for about 10 min. The reaction, which continued at 90 °C, was stopped after 24 h. The mixture at room temperature was neutralized by the addition of 37% HCl solution (1.65 mL, 20 mmol). The precipitate was filtered and washed with hot water (3 × 50 mL) to remove salts. Afterward, the residue was purified by washing with ethanol. The final oligo (EHPIMP) was dried in a vacuum oven at 80 °C for 24 h (Scheme 2).

(Yield: 49%. Color: dark black). IR (ν, cm^{-1}): 1654 (CH=N), 1581 (C=C aromatic), 1467 (–C=C–N), 1256 (C–O) 3061, 2975, (aromatic C–H) ^{1}H NMR (400 MHz, DMSO-d_6) δ (ppm): 11.33, (s, 1H, OH), 9.53 (s, 1H, OH), 8.31 (s, 1H, –N=CH), 7.93–6.21 (m, 7H, Ar–CH), 3.98 (OCH_2), 1.30 (CH_3); ^{13}C NMR (100 MHz, DMSO-d_6) δ (ppm): 165.36 (HC=N), 152.57, 150.47, 147.91, 142.40, 128.72, 128.48, 123.16, 121.56, 120.01, 114.30, 113.35 (C atoms on aromatic ring), 67.25 (OCH_2), 17.82 (CH_3).

Preparation of EHPIMP and oligo (EHPIMP) thin films

At first, the EHPIMP and the oligo (EHPIMP) were placed into separate tubes, taking 20 mg of each molecule. 1 mL of DMF was added to each tube and stirred at room temperature for 1 h. Additionally, the glass substrates were cleaned adequately with a piranha solution [mixture of 30% (vol) hydrogen peroxide and 70% (vol) concentrated sulfuric acid], and then the glass substrates were rinsed with water at ambient temperature [47, 48]. Preparation of EHPIMP and oligo (EHPIMP) films consisted of two steps, the first step was to make solutions and the second step involved casting the film. The prepared DMF solutions of the EHPIMP and the oligo (EHPIMP) were applied carefully onto clean glass slides using the drop casting, which is the solution process-based method, at room temperature (300 K), being careful to eliminate any air bubbles. This was then left overnight to evaporate the solvent. The final films of the EHPIMP and the oligo (EHPIMP) were prepared following this methodology which is depicted in Fig. 1. The thickness and exact dimensions of each film were determined by a digital micrometer (sensitivity: 0.001 mm), and the values were given as the average of five random measurements (Table 1).

Scheme 2 Synthesis of novel oligo (EHPIMP)

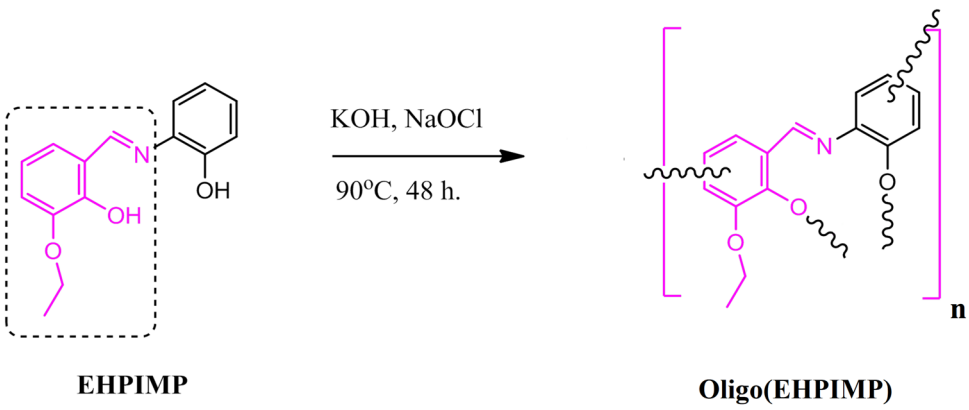

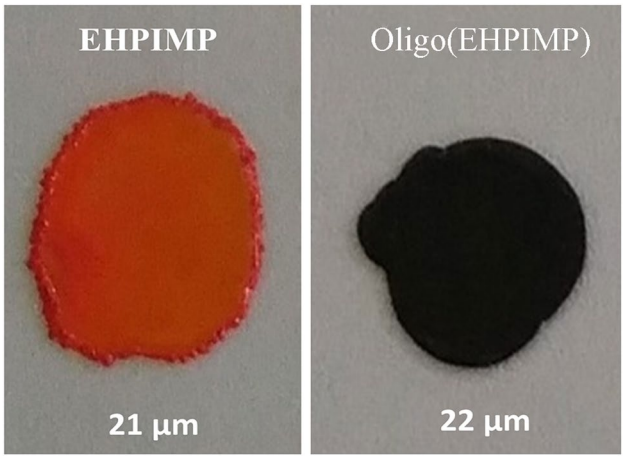

Fig. 1 Images of thin films

Table 1 The band gap values of thin films

Film thickness (µm)	EHPIMP 21	Oligo (EHPIMP) 22
E_g for Eq. 1 (eV)	2.183	1.370
E_g for Tauc equation (eV)	2.224	1.404
T_{avg}% (300–1100 nm)	10.2	23.3
T_{avg}% (380–780 nm) visible range	8.5	9.5

In vitro antioxidant activity assays

FRAP reducing method

Reducing antioxidant potentials of EHPIMP and oligo (EHPIMP) were determined by a modified FRAP method [49]. For this purpose EHPIMP, oligo (EHPIMP), and standard antioxidants (10–30 µg/mL) were prepared in 0.75 mL distilled water. One milliliter of potassium ferricyanide (1%) and 0.2 M sodium phosphate (pH 6.6) were added into each of the test samples. After 20 min incubation at 50 °C, 1 mL of trichloroacetic acid (TCA) (10%) was added to the mixtures. The reaction was completed by adding 0.25 mL of $FeCl_3$ (0.1%). A Shimadzu UV spectrophotometer (UV-1800, Japan) was used for the detection of their absorbances at 700 nm.

CUPRAC reducing method

Reducing Cu^{2+} ions to Cu^{+} ions mostly are related to antioxidant potential. CUPRAC method with a basic modification was used for this purpose [50]. The same amounts of (0.5 mL) neocuproine solution (7.5×10^{-3} M), $CuCl_2$ (0.01 M), and acetate buffer (1.0 M, pH 5.0) were added into separate test tubes, respectively. Then, EHPIMP, oligo (EHPIMP), and standard antioxidants (10–30 µg/mL) were added to the test tubes. The total volumes were completed to 4 mL with purified water. The samples were mixed well and stored for 30 min at room conditions. The absorbances at 450 nm were measured for all samples and standards.

ABTS radical scavenging method

The cation radical scavenging activities of the EHPIMP and the oligo (EHPIMP) were evaluated according to the ABTS (2,2′-azino-bis-3-ethylbenzothiazoline-6-sulfonic acid) method previously reported [51]. The ABTS cation radical solution has a dark blue color with a maximum absorbance at 734 nm. The cation radical solution was prepared by mixing 50 mL of ABTS (2 mM) with 50-mL potassium persulfate (2.45 mM) with a magnetic stirrer (12 h) at room temperature. The ratio of $ABTS^{\bullet+}$ and purified water was determined for the control solution to obtain around 0.9 ± 0.1 absorbance at 734 nm. The $ABTS^{\bullet+}$ solution was added to each EHPIMP, oligo (EHPIMP), and standard antioxidants (10–30 µg/mL). The absorbances of samples and standards were measured at 734 nm after vortexing and incubation in the dark.

DPPH radical scavenging method

DPPH (1,1-diphenyl-2-picryl-hydrazyl) method was used for the determination of free radical scavenging activities of EHPIMP and oligo (EHPIMP) [52, 53]. The reducing absorbance of the DPPH solution indicates the antioxidant potential of a substance. Then, EHPIMP, oligo (EHPIMP), and standard antioxidants (10–30 µg/mL) were prepared in 2-mL ethanol. One milliliter of DPPH radical solution (0.1 mM) was added to each sample. The absorbances of samples and standards were measured at 517 nm after vortexing and incubation in the dark.

Results and discussion

Synthesis and characterization

This research has been performed in three stages. In the first stage, the 2-ethoxy-6-(((2 hydroxyphenyl)imino)methyl) (EHPIMP) phenol was obtained. In the second stage, the new oligomer was carried out through oxidative polycondensation of EHPIMP. In the third stage, optical, morphological, and antioxidant properties of the synthesized EHPIMP and oligo (EHPIMP) were investigated.

The FTIR spectra of EHPIMP and oligo (EHPIMP) are shown in Fig. 2. In the IR spectra of EHPIMP, the bands at 3046, 2914 (aromatic C–H), 1590 cm^{-1} (C=C double bonds) and 1620 cm^{-1} (HC=N azomethine) are seen as distinctive

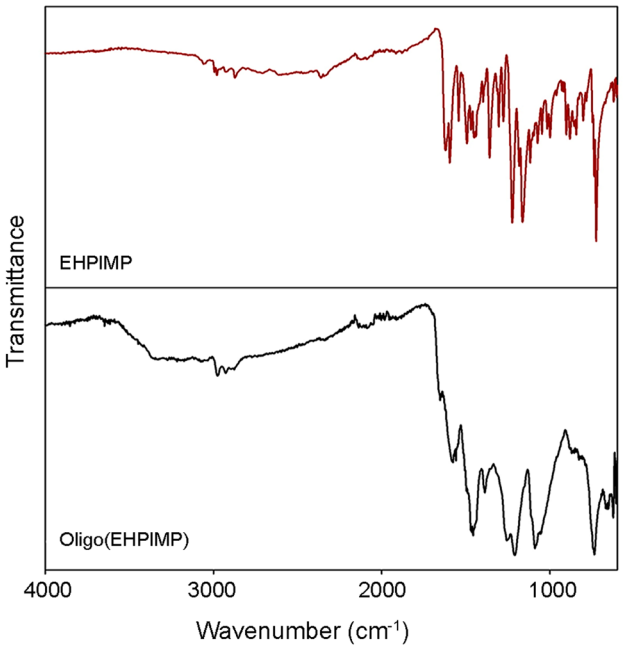

Fig. 2 FTIR spectra of EHPIMP and oligo (EHPIMP)

bands. The oligomer spectrum differs from the EHPIMP spectrum in terms of band strength and a decrease in wavelength due to the increase in molecular weight and polyconjugate structure after polycondensation. The FTIR spectrum of oligo (EHPIMP) showed bands at 1211 and 1254 cm^{-1}, which can be interpreted to phenolic C–O vibration [54]. Moreover, the azomethine stretching of the oligo (EHPIMP) shifted to 1654 cm^{-1}. The powerful band at 1579 cm^{-1} shows to the C=C stretching vibration of the aromatic ring. An important increment in the band intensity observed at 741 cm^{-1} for oligo (EHPIMP) indicates phenylene type couplings (C–C) that are dominant in polymer structure [55].

The hydroxyl and imine protons of the EHPIMP in ^{1}H NMR spectrum were seen at 14.14, 9.82 and 8.96 (–N=CH), respectively. When ^{1}H NMR spectra of the EHPIMP and the oligo (EHPIMP) are compared, the decrease of OH peaks of EHPIMP indicates that the hydroxyl groups in the polymerization may form C–O–C coupling with free radicals. It is apparent that after oxidative polycondensation, the signal of the oligo (EHPIMP) is broader than the EHPIMP due to the increasing molecular weight of oligo (EHPIMP). Furthermore, the decrease in the ratio of the integral height of aromatic protons to the integral height of the imine proton compared to the monomer in the oligomer shows aromatic ring protons attendance to the coupling reaction. When the ^{13}C NMR spectrum of the oligo (EHPIMP) and the EHPIMP are examined, imine carbons of the EHPIMP and the oligo (EHPIMP) are seen at 162 and 165.36 ppm, respectively. Moreover, aromatic carbons are monitored between the range of 152.38 and 116.94 ppm

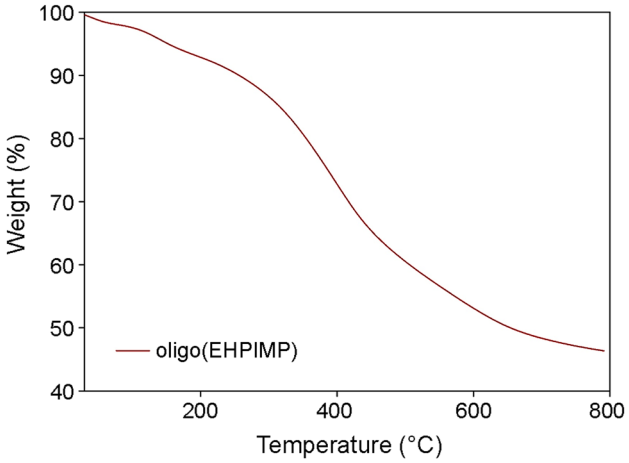

Fig.3 TGA curve of oligo (EHPIMP)

for the EHPIMP, and 152.57 and 113.35 ppm for the oligo (EHPIMP). On the other hand, the peaks at 63.99 and 15.62 ppm in the EHPIMP and the peaks at 63.99 and 15.62 in the oligo (EHPIMP) are identified as carbons of CH_2 and CH_3. The similarity of the ^{13}C NMR spectra of EHPIMP and oligo (EHPIMP) explains the preservation of EHPIMP structure in polymerization [56, 57].

The M_n and M_w and PDI values of the oligo (EHPIMP) determined by GPC were found as 1682 and 3231 g/mol, and 1.92, respectively.

The thermogravimetric analysis of the oligo (EHPIMP) was measured in the nitrogen medium, starting from room temperature up to 800 °C at a heating rate of 10 °C/min using a thermogravimetric technique (Fig. 3). While the weight loss of oligo (EHPIMP) started in the range of 30–108 °C due to the water molecules in the oligo (EHPIMP) structure, the weight loss at about 190 °C showed chemical C–O–C bonds. 50% weight loss of the oligo (EHPIMP) was also seen at 651 °C, and it left 46% residual at 800 °C. These results indicate a thermally stable oligo (EHPIMP) due to power C–C bonds and polyconjugation. Additionally, a linear decrease in weight loss was observed with an increase in temperature in the thermogram of the oligomer [58].

The optical properties of EHPIMP and oligo (EHPIMP) films

The Schiff-based polymers have attracted much attention due to the optical properties and electronic applications. As shown by the absorbance graphs of the EHPIMP and oligo (EHPIMP) film (Fig. 4), the value absorbed by EHPIMP was greater than the value absorbed by oligo (EHPIMP) and accordingly the EHPIMP absorbed light at a lower wavelength, while oligo (EHPIMP) absorbed light at a higher wavelength.

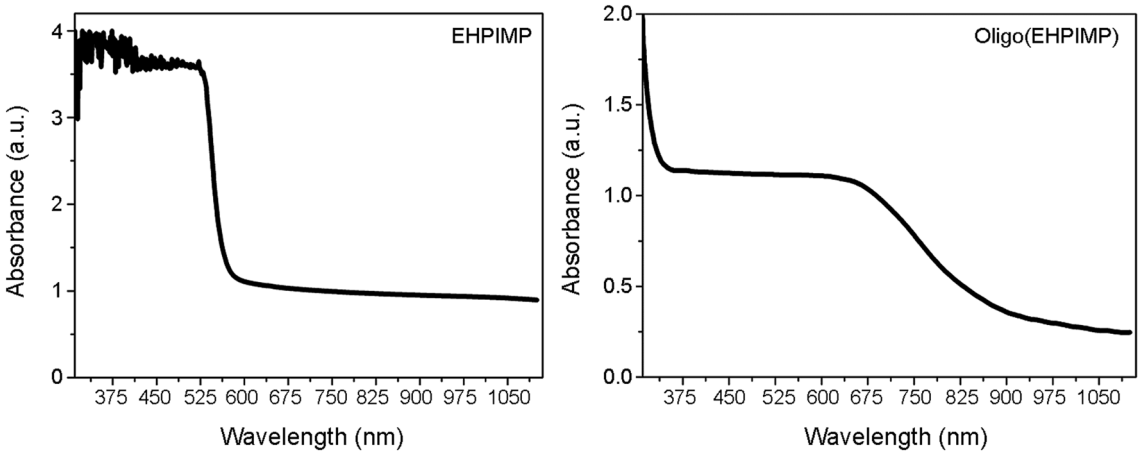

Fig. 4 The absorbance graph as a function of wavelength in thin films

In Fig. 4, it was observed that EHPIMP and oligo (EHPIMP) films absorbed more in the range of 520–582 nm and 642–905 nm, respectively. The oligo (EHPIMP) film's absorbance value remained constant after a certain amount of wavelength. Contrary to the oligo (EHPIMP), for the EHPIMP film, it was observed that the absorbance was wavy in the range of 328–518 nm. According to Fig. 4, the EHPIMP was observed to be absorbed by near-ultraviolet and near-visible region, while the oligo (EHPIMP) was observed to absorb near-ultraviolet, visible and near-infrared region. It is known that conjugated materials begin to absorb at high wavelengths as conjugation increases. At high wavelengths of EHPIMP and oligo (EHPIMP) molecules (around 580 nm and 920 nm, respectively) started to absorb due to high conjugation. When the EHPIMP was turned into oligo (EHPIMP), the number of the repeating units increased which caused an increase in conjugation. Hence, the absorption value was shifted to a higher wavelength. λ_{onset} values of coated films were calculated from the absorbance edges [59]. The absorbance edges of the 21-μm-coated film of the EHPIMP and 22-μm-coated film of the oligo (EHPIMP) were found as 568 nm and 905 nm, respectively. The optical band gap (E_g) of the EHPIMP and the oligo (EHPIMP) films were calculated from the absorption spectra using Eq. 1 given below (Table 1) [60].

$$E_g = 1240/\lambda_{onset}. \quad (1)$$

The optical band gap of the EHPIMP (21 μm) and oligo (EHPIMP) (22 μm) films were calculated as 2.183 eV and 1.370 eV, respectively.

The transmittance graphs for the EHPIMP and the oligo (EHPIMP) films are observed in Fig. 5. The transmittance values of the EHPIMP and oligo (EHPIMP) films were observed in the range of 0–12% and 0–56%, respectively. The average transmittance values in the range of 300–1100 nm of the EHPIMP (21 μm) and the oligo (EHPIMP) (22 μm) films were found as 10.2 and 23.3%, respectively (Table 1).

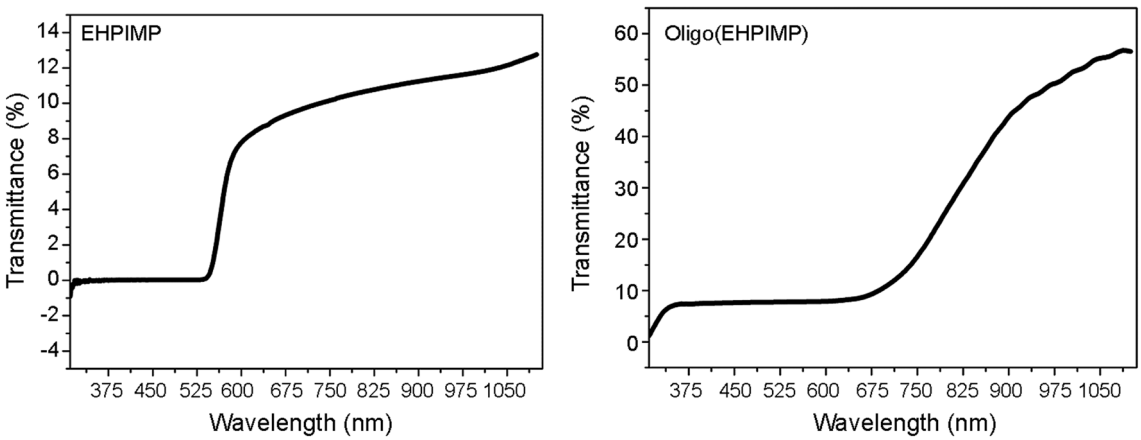

Fig. 5 The transmittance graph as a function of wavelength in thin films

Similarly, the average transmittance values of the films were determined as 8.5% and 9.5% in the visible range (between 380 and 780 nm), respectively (Table 1).

The band gap values of semiconductor materials for optoelectronic and solar cells are of great importance [61]. To find the band gap of EHPIMP and oligo (EHPIMP) films, Tauc equation was used to obtain photon energy with $(\alpha h\nu)^2$ [62, 63] (Fig. 6).

It was observed that the band gap values of the Schiff-based films were found to be 2.224 for the EHPIMP (21 µm) and 1.404 eV for the oligo (EHPIMP) (22 µm), respectively. The Tauc equation and the values found in Eq. 1 were found to be almost compatible with each other (Table 1). The band gap values of the EHPIMP and the oligo (EHPIMP) were calculated with the two equations, and it was determined that these conjugated materials had low band gap values. The conjugated molecules with a band gap of less than 1.6 eV are known to be more suitable for ambipolar field effect transistors (FETs), organic photovoltaics (OPV) and photodetectors (PDs) [64–66]. In this study, the E_g values of oligo (EHPIMP) were found to be very low. The reason why the differences in band gap values between EHPIMP and oligo (EHPIMP) are such large can be explained by the fact that the interaction between alternating donors and acceptors results in a compressed band gap [67]. Besides, in some other studies, the band gap values of conjugated molecules for photovoltaic applications were reported as between 1.6 and 2.5 eV [68, 69]. In this case, it can be said that EHPIMP and oligo (EHPIMP) are convenient for photovoltaic applications, because their band gap values were found between 1.6 and 2.5 eV. In this study, the oligo (EHPIMP) organic semiconductor, with a low band gap, was easily obtained. The oligo (EHPIMP) with a low band gap was obtained without complex formation and doping makes this study useful for photovoltaic applications.

Morphological properties of EHPIMP and oligo (EHPIMP)

AFM is a device that can measure surface topography from an angstrom to 100–150 microns. The atomic force microscope is the system with a nano-sized type that is moved on the surface of the sample and it obtains the image of the surface by detecting the force applied to the atoms on the surface [70].

Figures 7 and 8 show two-dimensional and three-dimensional 5µ x 5µ phase images of the EHPIMP and oligo (EHPIMP) films. When the phase images are examined, it is seen that EHPIMP film is generally homogeneous, smooth, and small grained. The differences in color represent the different heights in the images [71]. For example, the black ones represent the valleys, and the white ones represent the hills. From the surface morphology of the compound, the grains of different sizes and heights seem intertwined. In the measurement, the roughness value, Ra, was measured as 46.63 nm, and the roughness value, Rq, was 55.14 nm as shown in Table 2.

When the phase images of the oligo (EHPIMP) film are examined, it is seen that the film has a homogeneous, smooth, fine-grained structure and the maximum height among the pits and valleys formed on the surface is 44 nm. The roughness value, Ra, was measured as 8.28 nm, and the roughness value, Rq, was 9.96 nm. Morphological examinations of three Schiff-bases have been studied by Derkowska-Zielinska et al. [72]. According to their findings, roughness parameters (roughness average and surface roughness, respectively) calculated from AFM images were found to be 1.76 nm and 2.25 nm for Schiff-base with 2-(2-pyridyl)ethylamine, 8.84 nm and 10.4 nm for Schiff-base with cyclohexanediamine, and Ra = 4.99 nm and 6.28 nm for Schiff-base with cyclohexanediamine with NO_2 group. These values are

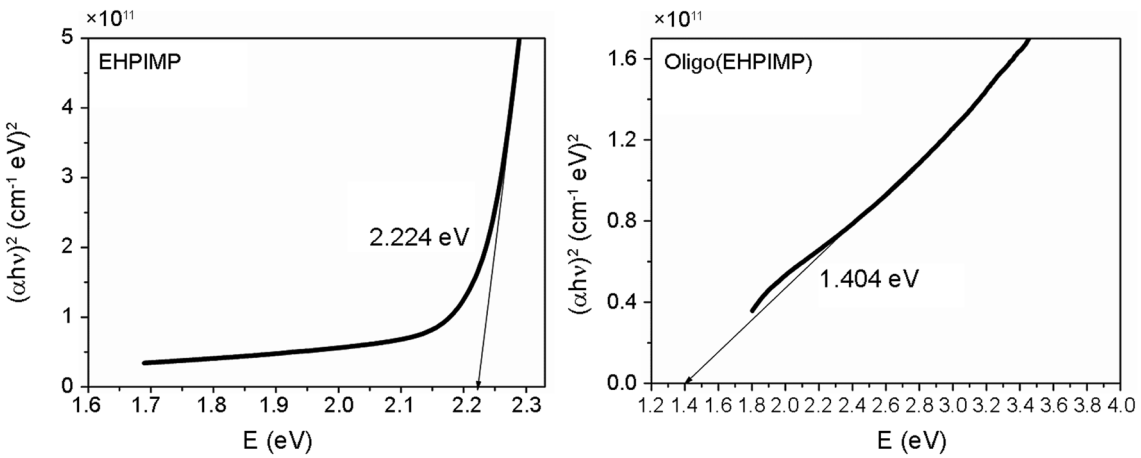

Fig. 6 The graph of $(\alpha h\nu)^2$ with photon energy of thin films

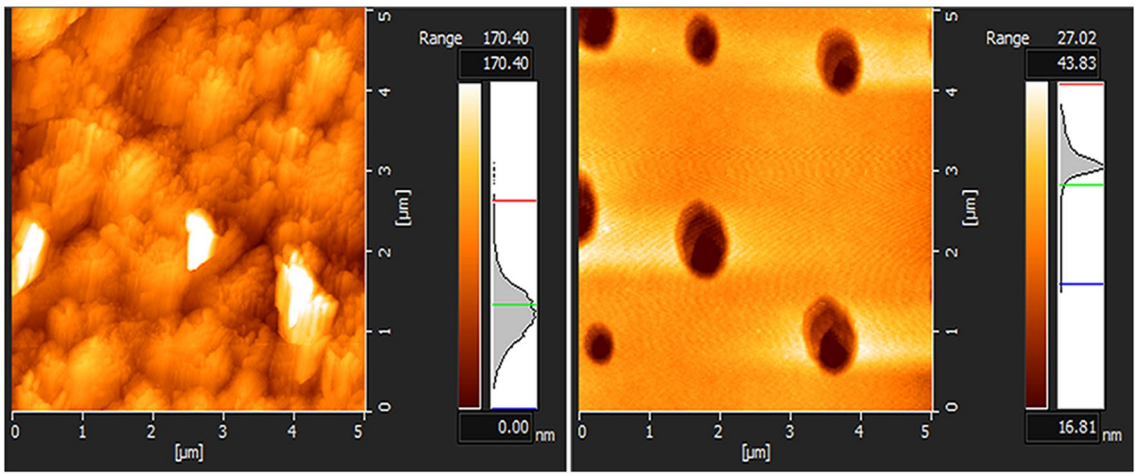

Fig. 7 2D AFM images of thin films

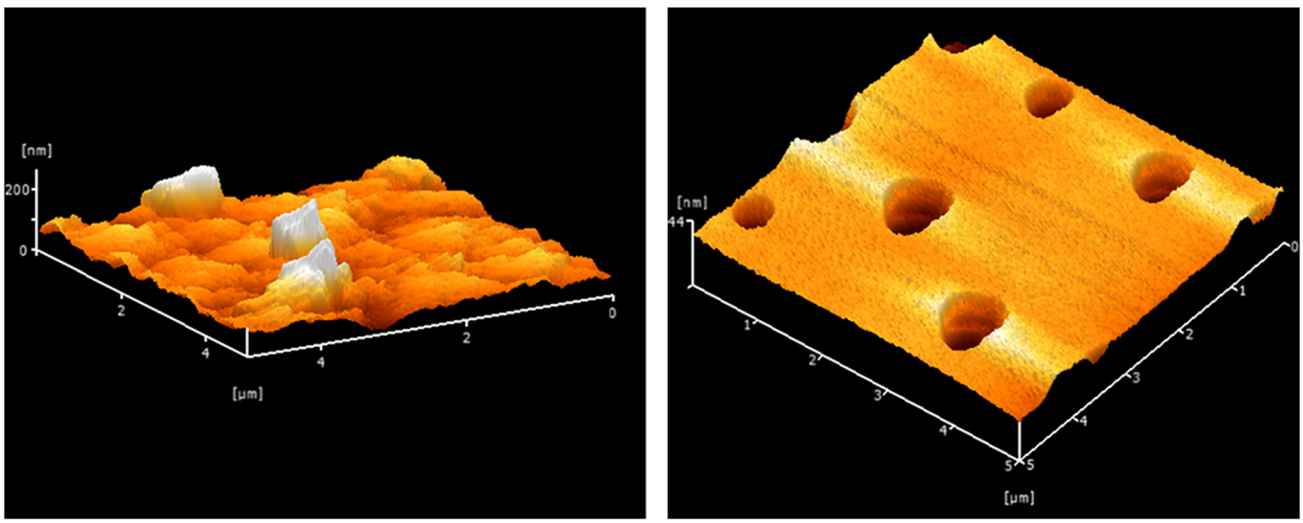

Fig. 8 3D AFM images of thin films

Table 2 AFM surface parameters of thin films

	EHPIMP	Oligo (EHPIMP)
Roughness average (Ra)	46.63	8.28
Surface roughness (Rq)	55.14	9.96
Peak (Rp)	124.50	9.48
Valley (Rv)	62.99	24.90
Peak-Valley (Rt)	187.49	34.38

quite reasonable when compared to the surface parameters of the oligo (EHPIMP) thin film we have obtained.

Antioxidant studies on EHPIMP and oligo (EHPIMP)

The antioxidant capabilities of the samples were investigated by four in vitro methods. FRAP and CUPRAC methods were used for determining reducing antioxidant characterization as well as ABTS and DPPH methods used for determining radical scavenging characterization.

The reducing ferric ions indicate the antioxidant-reducing potential of a substance. Antioxidant molecules usually transfer a single electron to act as a reducing agent. According to the FRAP assay, the ferric reducing capabilities of the samples and standards decreased as BHA, BHT, ascorbic acid, the EHPIMP, tocopherol, and the oligo (EHPIMP), respectively. The increasing absorbance of a sample indicates its reducing activity potential. The data of this method

are graphed in Fig. 9. The reducing amount of the EHPIMP was higher than the tocopherol and very close to the other standards. However, the oligo (EHPIMP) showed the lowest reducing ferric ions activity among the standards and tested samples.

Similarly, reducing cupric ions potential of a sample indicates its antioxidant potential. The cupric reducing capabilities of the samples and standards were decreased as BHT, BHA, the oligo (EHPIMP), the EHPIMP, tocopherol, and ascorbic acid, respectively. The samples were shown effective cupric ions reducing potential as indicated in Fig. 10. The reducing amounts of the oligo (EHPIMP) and the EHPIMP were higher than those of tocopherol and ascorbic acid but lower than those of the other standard antioxidant compounds.

Antioxidant compounds have good capabilities of single electron transfer or hydrogen atom transfer to reactive or radical species. Thus, antioxidants can scavenge radical species that make them more stable and unreactive compounds. The present study determined the radical scavenging antioxidant potential of the samples and standards by in vitro DPPH and ABTS assays.

The IC_{50} values (concentration of a sample that scavenges 50% of radicals) and scavenging percentages (%) for ABTS and DPPH radicals are given in Table 3. According to the obtained results of ABTS and DPPH methods, effective radical scavenging antioxidant activities of EHPIMP and oligo (EHPIMP) were detected.

The ABTS radical scavenging percentages of the samples and standards at the same concentration (30 µg/mL) decreased in the order of ascorbic acid (93.5 ± 2.9), oligo (EHPIMP) (89.9 ± 1.1), tocopherol (83.4 ± 4.7), BHT (79.4 ± 18.1), EHPIMP (78.6 ± 16.3), BHA (73.4 ± 7.6), and trolox (68.4 ± 14.7).

DPPH radical scavenging percentages of samples at the same concentration (30 µg/mL) decreased in the order of BHA (63.6 ± 9.8), ascorbic acid (63.6 ± 18.9), EHPIMP (51.0 ± 9.7), BHT (47.2 ± 12.7), tocopherol (44.4 ± 23.9), trolox (38.1 ± 17.6), and oligo (EHPIMP) (33.4 ± 6.9).

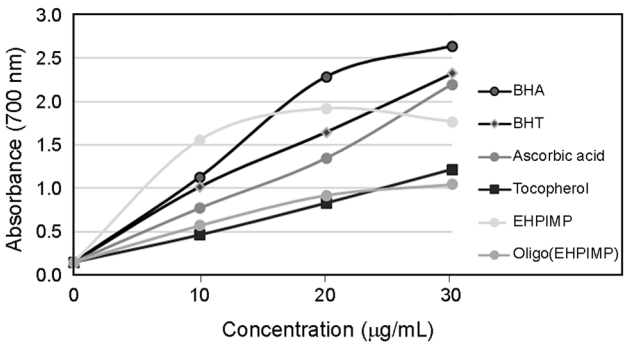

Fig. 9 Ferric reducing antioxidant potentials of samples and standard compounds

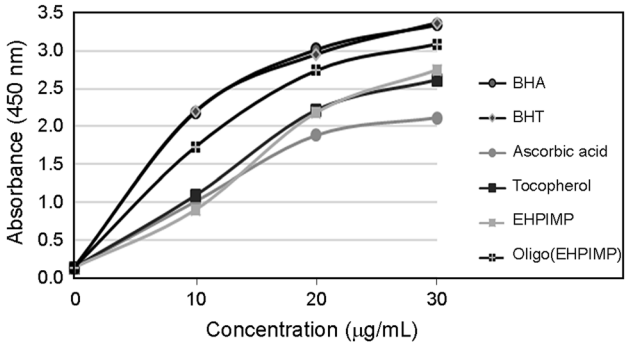

Fig. 10 Cupric reducing antioxidant capacities of samples and standard compounds

Conclusion

The novel oligo (EHPIMP) with a low band gap was synthesized and characterized. Films of the obtained EHPIMP and the oligo (EHPIMP) were prepared and their optical properties were examined. It was observed that the surface roughness values decreased with the transition from EHPIMP film to poly-oligo (EHPIMP). This smoothness is essential for the reliability, processability, and interfacing of such films. The band gap values of the EHPIMP and the oligo (EHPIMP) were calculated both with Tauc equation and using the wavelength peak from the absorption spectrum and it was found to be very low the band gap values and the resulting data were compatible with each other. Thus, they were suitable for photovoltaic applications. The results of in vitro antioxidant methods showed that the EHPIMP and oligo (EHPIMP) have effective reducing antioxidant potentials and radical

Table 3 Determination of half maximal concentrations (IC_{50}) and scavenging percentages (%) of samples and standards for ABTS and DPPH radicals

Sample	ABTS scavenging		DPPH scavenging	
	IC_{50}*	%**	IC_{50}*	%**
BHA	14.2 ± 8.5	73.4 ± 7.6	15.2 ± 5.6	63.6 ± 9.8
BHT	14.1 ± 10.3	79.4 ± 18.1	20.3 ± 5.4	47.2 ± 12.7
Ascorbic acid	10.6 ± 5.1	93.5 ± 2.9	15.0 ± 3.5	63.6 ± 18.9
Tocopherol	16.3 ± 11.6	83.4 ± 4.7	22.9 ± 1.0	44.4 ± 23.9
Trolox	11.8 ± 5.4	68.4 ± 14.7	25.8 ± 1.2	38.1 ± 17.6
EHPIMP	13.2 ± 6.6	78.6 ± 16.3	18.8 ± 6.4	51.0 ± 9.7
Oligo (EHPIMP)	11.1 ± 5.6	89.9 ± 1.1	28.7 ± 9.3	33.4 ± 6.9

*Sample concentration to scavenge 50% of radicals

**Scavenging percentages of samples at 30 µg/mL

scavenging activities. The EHPIMP and oligo (EHPIMP) materials having low optical band gap and good antioxidant effects might be good candidates for optoelectronic devices and drug design.

Acknowledgements We thank Dr. Adem Korkmaz for her contribution in chemical synthesis.

Funding The authors received no specific funding for this work.

Compliance with ethical standards

Conflict of interest The authors confirm that this article content has no conflict of interest.

References

1. Grigoras M, Catanescu CO (2004) Imine polymers and polymers. J Macromol Sci Part C Polym Rev 44:131–173
2. Cantón-Díaz AM, Muñoz-Flores BM, Moggio I, Arias E, De León A, García-López MC, Santillán R, Ochoa ME, Jiménez-Pérez VM (2018) One-pot microwave-assisted synthesis of organotin Schiff bases: an optical and electrochemical study towards their effects in organic solar cells. N J Chem 42:14586–14596
3. Mahadevi P, Sumathi S (2020) Mini review on the performance of Schiff base and their metal complexes as photosensitizers in dye-sensitized solar cells. Synth Commun 50:2237–2249
4. Wang Y, Ye W, Yang X, Rezaee E, Shan H, Yang S, Cai S, Jia-Hong Pan JH, Xu J, Xu ZX (2020) Hole transport layers based on metal Schiff base complexes in perovskite solar cells. Synth Metal 259:116248
5. Bhatt KD, Upadhyay SV (2020) Review on Schiff base: a Scrupulous binding detector for metal ions. Org Chem Plus 1:29–33
6. Kaya I, Ayten B, Şenol D (2018) Syntheses of poly(phenoxy-imine)s anchored with carboxyl group: characterization and photovoltaic studies. Opt Mater 7:421–431
7. Shaalan N, Laftah N, El-Hiti GA, Alotaibi MH, Muslih R, Ahmed DS, Yousif E (2018) Poly(vinyl chloride) photostabilization in the presence of Schiff bases containing a thiadiazole moiety. Molecules 23:913
8. Ibrahim EMM, Abdel-Rahman LH, Abudief AM, Hamdan SK (2018) The electric and thermoelectric properties of Cu(II)-Schiff base nano-complexes. Phys Scripta 93:055801
9. Zhang J, Xu L, Wong WY (2018) Energy materials based on metal Schiff base complexes. Coord Chem Rev 355:180–198
10. Shokohi-Pour Z, Chiniforoshan H, Sabzalian MR, Esmaeili SA (2018) Cobalt (II) complex with novel unsymmetrical tetradentate Schiff base (ON) ligand: in vitro cytotoxicity studies of complex, interaction with DNA/protein, molecular docking studies, and antibacterial activity. J Biomol Struct Dyn 36:532–549
11. Kamaci M, Kaya I (2018) Melamine-based poly(azomethine) hydrogels: mechanical, biodegradability, drug loading and antibacterial properties. Eur Polym J 108:107–115
12. Petrova P, Chochkova M, Veleva O, Karadjov M (2020) Schiff bases chelate sorbents for seperation and concentration of Pt from sea water and spent automotive catalysts. J Chem Tech Metall 55:691–697
13. Fernández N, Sánchez-Fontecoba P, Castillo-Martínez E, Carretero-González J, Rojo T, Armand M (2018) Polymeric redox-active electrodes for sodium-ion batteries. Chemsuschem 11:311–319
14. Channa AM, Memon SQ, Khuhawar MY, Baytak S (2020) Synthesis of trifluoroacetylacetone resin through Schiff's base reaction for treatment of cadmium-contaminated water. Arab J Sci Eng 45:4765–4772
15. Ikemura K, Kadoma Y, Endo T (2011) A review of the developments of self-etching primers and adhesives—effects of acidic adhesive monomers and polymerization initiators on bonding to ground, smear layer-covered teeth. Dent Mater J 30:769–789
16. Kumar K-G, John K-S (2006) Complexation and ion removal studies of a polystyrene anchored Schiff base. React Funct Polym 66:1427–1433
17. Hasnaoui A, Idouhli R, Nayad A, Ouahine H, Khadiri ME, Abouelfida A, Elfirdoussi L, Ali MA (2020) Di-nuclear water-soluble oxovanadium (V) Schiff base complexes: electrochemical properties and catalytic oxidation. Inorg Chem Commun 119:108134
18. Xue J, Uchida S, Rand BP, Forrest SR (2004) Asymmetric tandem organic photovoltaic cells with hybrid planar-mixed molecular heterojunctions. Appl Phys Lett 85:5757–5759
19. Yang Z, Moffa M, Liu Y, Li H, Persano L, Camposeo A, Saija R, Antonia Latì M, Maragò OM, Pisignano D, Nam CY, Zussman E, Rafailovich M (2018) Electrospun conjugated polymer/fullerene hybrid fibers: photoactive blends, conductivity through tunneling-AFM, light scattering, and perspective for their use in bulk-heterojunction organic solar cells. J Phys Chem C 122:3058–3067
20. Hindson J-C, Ulgut B, Friend R-H, Greenham N-C, Norder B, Kotlewski A, Dingemans T-J (2010) All-aromatic liquid crystal triphenylamine-based poly(azomethine)s as hole transport materials for opto-electronic applications. J Mater Chem 20:937–944
21. Bucella SG, Luzio A, Gann E, Thomsen L, McNeill CR, Pace G, Perinot A, Chen Z, Facchetti A, Caironi M (2015) Macroscopic and high-throughput printing of aligned nanostructured polymer semiconductors for MHz large-area electronics. Nat Commun 6:1–10
22. Erdoğan E, Kundakçı M (2019) Influence of substrate and substrate temperature on the structural, optical and surface properties of InGaN thin films prepared by RFMS method. Microelectron Eng 207:15–18
23. Erdoğan E, Kundakçı M (2019) Changes of the physical properties of sputtered InGaN thin films under small nitrogen gas flow variations. J Electron Mater 48:2924–2931
24. Martin BD (2017) U.S. Patent No. 9,738,609. Washington DC: U.S. Patent and Trademark Office
25. Chénais S, Forget S (2012) Recent advances in solid-state organic lasers. Polym Int 61:390–406
26. Hide F et al (1996) Semiconducting polymers: a new class of solid-state laser materials. Science 273:1833–1836
27. Kamacı M, Kaya İ (2016) New low-band gap polyurethanes containing azomethine bonding: photophysical, electrochemical, thermal and morphological properties. J Taiwan Inst Chem Eng 59:536–546
28. Davy NC, Sezen-Edmonds M, Gao J, Lin X, Liu A, Yao N, Kahn A, Loo YL (2017) Pairing of near-ultraviolet solar cells with electrochromic windows for smart management of the solar spectrum. Nat Energy 2:1–11
29. Chen Q, Ye F, Lai J, Dai P, Lu S, Ma C, Chen L (2017) Energy band alignment in operando inverted structure P3HT:PCBM organic solar cells. Nano Energy 40:454–461
30. Sandanayaka AS, Matsushima T, Bencheikh F, Yoshida K, Inoue M, Fujihara T, Goushi K, Ribierre JC, Adachi C (2017) Toward continuous-wave operation of organic semiconductor lasers. Sci Adv 3:e1602570
31. Zhang CH, Yu PP, Tan WY, Luo D, Wang LP, Xia Y, Liu CC, Cao Y (2019) An easily and environmentally friendly accessible small-molecule acetylenic donor for organic solar cells. Dye Pigment 160:983–988
32. Wang H, Wu J, Zhang Y, Song J, Chen L, Xiao Y, Qu J, Wong WY (2020) Achieving efficient green-solvent-processed organic solar

cells by employing ortho-ortho perylene diimide dimer. Organ Electron 83:105732
33. Wu C, Kim TW, Guo T, Li F (2017) Wearable ultra-lightweight solar textiles based on transparent electronic fabrics. Nano Energy 32:367–373
34. Ramanujam PS, Hvilsted S, Ujhelyi F, Koppa P (2001) Physics and technology of optical storage in polymer thin films. Synth Met 124:145–150
35. Boyle AJ, Weems AC, Hasan SM, Nash LD, Monroe MBB, Maitland DJ (2016) Solvent stimulated actuation of polyurethane-based shape memory polymer foams using dimethyl sulfoxide and ethanol. Smart Mater Struct 25:075014
36. Yiğit B, Yiğit M, Taslimi P, Gök Y, Gülçin İ (2018) Schiff bases and their amines: synthesis and discovery of carbonic anhydrase and acetylcholinesterase enzymes inhibitors. Arch Pharm 351:1800146
37. Shanty AA, Mohanan PV (2018) Heterocyclic Schiff bases as non toxic antioxidants: solvent effect, structure activity relationship and mechanism of action. Spectrochim Acta Part A Mol Biomol Spectrsc 192:181–187
38. Orabi EA (2018) Tautomerism and antioxidant activity of some 4-acylpyrazolone-based Schiff bases: a theoretical study. RSC Adv 8:30842–30850
39. Hassib HB, Issa YM, Mohamed WS (2008) Electrical and thermal studies on some acetylacetone and benzoylacetone-arylhydrazones. J Therm Anal Calorim 92:775–782
40. Hassib H, Razik AA (2008) Dielectric properties and AC conduction mechanism for 5,7-dihydroxy-6-formyl-2-methylbenzo-pyran-4-one bis-Schiff base. Solid state Commun 147:345–349
41. Cetin A, Korkmaz A, Kaya E (2018) Synthesis, characterization and optical studies of conjugated Schiff base polymer containing thieno [3, 2-b] thiophene and 1, 2, 4-triazole groups. Opt Mater 76:75–80
42. Al-Sahlane TQ, Al-Amery MH (2018) Synthesis, characterization, antioxidant and anticancer human studies of new metal ion complexes of poly Schiff base derived from 4-aminoacetophenone with salicylaldehyde and 4-bromoaniline. Synthesis 11:489–493
43. Trávníček Z, Štarha P, Čajan M, Dvořák Z (2019) A half-sandwich TaV dichlorido complex containing an O, N, O′-tridentate Schiff base ligand: synthesis, crystal structure and in vitro cytotoxicity. Acta Crystallogr Sect C Struct Chem 75:248–254
44. Bursal E, Taslimi P, Gören AC, Gülçin İ (2020) Assessments of anticholinergic, antidiabetic, antioxidant activities and phenolic content of *Stachys annua*. Biocatal Agric Biotech 28:101711
45. Alsalim TA, Hadi JS, Ali ON, Abbo HS, Titinchi SJ (2013) Oxidation of benzoin catalyzed by oxovanadium (IV) Schiff base complexes. Chem Cent J 7:3
46. Mart H (2006) Oxidative polycondensation reaction. Des Monom Polym 9:551–588
47. Korkmaz A, Cetin A, Kaya E, Erdoğan E (2018) Novel polySchiff base containing naphthyl: synthesis, characterization, optical properties and surface morphology. J Polym Res 25:1–8
48. Cetin A, Korkmaz A, Bildirici I (2018) A novel poly-pyrazole-based thin film: synthesis, characterization, optical and morphological properties. Colloid Polym Sci 296:1249–1257
49. Dastan T, Kocyigit UM, Dastan SD, Kilickaya PC, Taslimi P, Cevik O, Koparir M, Orek C, Gulcin I, Cetin A (2017) Investigation of acetylcholinesterase and mammalian DNA topoisomerases, carbonic anhydrase inhibition profiles, and cytotoxic activity of novel bis(α-aminoalkyl) phosphinic acid derivatives against human breast cancer. J Biochem Mol Toxic 31:e21971
50. Silinsin M, Bursal E (2018) UHPLC–MS/MS phenolic profiling and in vitro antioxidant activities of *Inula graveolens* (L.) Desf. Nat Prod Res 32:1467–1471
51. Bener M, Şen FB, Apak R (2018) Heparin-stabilized gold nanoparticles-based CUPRAC colorimetric sensor for antioxidant capacity measurement. Talanta 187:148–155
52. Taslimi P, Gulçin I (2018) Antioxidant and anticholinergic properties of olivetol. J Food Biochem 42:e12516
53. Bursal E, Boğa E (2018) Polyphenols analysed by UHPLC–ESI–MS/MS and antioxidant activities of molasses, acorn and leaves of oak (Quercus robur subsp. pedunculiflora). Prog Nutr 20:167–175
54. Kaya I, Yıldırım M, Avcı A (2010) Synthesis and characterization of fluorescent polyphenol species derived from methyl substituted aminopyridine based Schiff bases: the effect of substituent position on optical, electrical, electrochemical, and fluorescence properties. Synth Met 160:911–920
55. Oguchi T, Tawaki S, Uyuma H, Kobayashi S (1999) Soluble polyphenol. Macromol Rapid Commun 20:401–403
56. Ayyagari MS, Marx KA, Tripathy SK, Akkara JA, Kaplan DL (1995) Controlled free-radical polymerization of phenol derivatives by enzyme-catalyzed reactions in organic solvents. Macromolecules 28:5192–5197
57. Özbülbül A, Mart H, Tunçel M, Serin S (2006) A new soluble Schiff base polymer with a double azomethine group synthesized by oxidative polycondensation. Des Monom Polym 9:169–179
58. Ng HM, Saidi NM, Omar FS, Ramesh K, Ramesh S, Bashir S (2020) Thermogravimetric analysis of polymers. Encycl Polym Sci Technol. https://doi.org/10.1002/0471440264.pst667
59. Kaya I, Kamacı M (2018) Synthesis, optical, and thermal properties of polyimides containing flexible ether linkage. J Appl Polym Sci 135:46573
60. Kamaci M, Kaya I (2014) Photophysical, electrochemical, thermal and morphological properties of polyurethanes containing azomethine bonding. J Macromol Sci Part A 51:805–819
61. Souri D, Sarfehjou M, Khezripour AR (2018) The effect of ambient temperature on the optical properties and crystalline quality of ZnSe and ZnSe: Cu NCs grown by rapid microwave irradiation. J Mater Sci Mater Electron 29:3411–3422
62. Cetin A, Korkmaz A, Erdoğan E, Kösemen A (2019) A study on synthesis, optical properties and surface morphological of novel conjugated poly-pyrazole films. Mater Chem Phys 222:37–44
63. Cetin A, Korkmaz A (2018) Synthesis, optical and morphological properties of novel pyrazole-based polyamide film. Opt Mater 85:79–85
64. Li G, Chang WH, Yang Y (2017) Low-bandgap conjugated polymers enabling solution-processable tandem solar cells. Nat Rev Mater 2:1–13
65. Wu W, Liu Y, Zhu D (2010) π-Conjugated molecules with fused rings for organic field-effect transistors: design, synthesis and applications. Chem Soc Rev 39:1489–1502
66. Roncali J (1997) Synthetic principles for bandgap control in linear π-conjugated systems. Chem Rev 97:173–206
67. Rasmussen S (2013) Low-bandgap polymers. In: Kobayashi S, Müllen K (eds) Encyclopedia of polymeric nanomaterials. Springer, Berlin, Heidelberg, pp 1155–1166
68. Hou J, Chen HY, Zhang S, Chen RI (2009) Synthesis of a low band gap polymer and its application in highly efficient polymer solar cells. J Am Chem Soc 131:15586–15587
69. Wu CG, Hsieh CW, Chen DC, Chang SJ, Chen KY (2005) Low band gap-conjugated polymer derivatives. Synth Met 155:618–622
70. Kumar BR, Rao TS (2012) AFM studies on surface morphology, topography and texture of nanostructured zinc aluminum oxide thin films. Dig J Nanomat Biostruct 7:1881–1889
71. Raposo M, Ferreira Q, Ribeiro PA (2007) A guide for atomic force microscopy analysis of soft-condensed matter. Mod Res Educ Top Microsc 1:758–769
72. Derkowska-Zielinska B, Barwiolek M, Cassagne C, Boudebs G (2020) Nonlinear optical study of Schiff bases using Z-scan technique. Opt Laser Tech 124:105968